37

TID-25548

A Facsimile Report

Reproduced by
UNITED STATES
ATOMIC ENERGY COMMISSION
Division of Technical Information
P.O. Box 62 Oak Ridge, Tennessee 37830

SGT.64243R

TID-25548

MEASUREMENTS OF TRANSITION PROBABILITIES IN SOME MIDDLE WEIGHT NUCLEI

by

RICHARD ANDREW KUEBBING

Submitted in partial fulfillment of the requirements

for the Degree of Doctor of Philosophy

Department of Physics

CASE WESTERN RESERVE UNIVERSITY

January 1970

MEASUREMENTS OF TRANSITION PROBABILITIES
IN SOME MIDDLE WEIGHT NUCLEI

Abstract

by

RICHARD ANDREW KUEBBING

The level schemes of Nb^{92} and Nb^{94} have been studied via the (p,n) reaction on separated zirconium targets. The pulsed beam of the ORNL 6 MeV Van de Graaff was used to measure the lifetimes of excited states of these nuclei. The 140.4 keV state in Nb^{94} has been found to have a half-life of (36.8 $\pm$ 0.4) nanoseconds by measuring the decay of the 99.4 keV gamma ray after the production of the state by the pulsed beam. The 226 keV state in Nb^{92} has been found to have a half-life of (5.2 $\pm$ 0.7) microseconds by measuring the decay of the 90.7 keV gamma ray in the same manner. The spins and parities of these states imply that they should be E1 transitions. They are slower however than Weisskopf estimates by factors of 8×10^{-6} and 6×10^{-8} respectively. A simple explanation of this hindrance is proposed by invoking the shell model.

A study of the decay of Br^{80} to the levels of Kr^{80} has been made to test the phonon character of the 0^+ excited state of Kr^{80}. A search was made for the decay of this state by E0 conversion

electron as predicted by Reiner. The energy spectrum of electrons from this source in coincidence with other radiation was measured but no peak was seen. Methods for increasing the sensitivity of the experiment are discussed.

ACKNOWLEDGMENTS

This thesis is dedicated to all who have helped its author pursue learning through Physics. Professors Stefan Machlup, Paul Zilsel and Leonard Kisslinger at Western Reserve University have provided him with a basic knowledge and understanding of theory by their dedicated teaching. The author is indebted to Dr. Karl Casper who introduced him to experimental nuclear physics and whose patient direction and assistance during the course of this thesis is much appreciated. The experimental measurements and data analysis were performed while the author was a guest at the Chemistry Division of the Oak Ridge National Laboratory, which is operated by Union Carbide Corporation for the U. S. Atomic Energy Commission. The author and his research were patiently guided by Drs. Gene Eichler and Kirk Dickens. Their interest in both have brought them to their present stages of perfection. The author gratefully shares his joy of accomplishment with them. The hospitality of the Nuclear Chemistry Group at ORNI is very much appreciated. Discussions with Drs.Dave O'Kelley and Noah Johnson have been very helpful. The companionship, scientific and otherwise, of his fellow graduate students and post-doctoral, Len Finkel, Dr. Lee Riedinger, Dr. Richard Hagenauer, Dr. Robert Lanier and Tony Kluk is recognized and thanks rendered. The aid of Mr. Ron McCann in processing the bromine data is gratefully acknowledged.

For the actual production of the thesis the author gratefully acknowledges Mrs. Jeane Fullerton and Mrs. Ruby Burrell for their speedy and accurate typing, and Mr. William Dunlap for his excellent drafting of many of the figures.

For financial support the author is indebted to the National Aeronautics and Space Administration and the University Participation Office of the Oak Ridge Associated Universities for pre-doctoral fellowships; and to the Chemistry Division for the use of its facilities and the help of its staff.

A large measure of thanks is owed to my family and my wife's family whose support has been crucial, especially in the last year. Last but not least to my wife, Sharyn, who in sickness and in health has been an inspiration.

TABLE OF CONTENTS

LIST OF FIGURES

LIST OF TABLES

CHAPTER I

A. INTRODUCTION

Since Rutherford[1] postulated the nucleus to explain the alpha particle scattering data of Gieger and Marsden,[2,3] much progress has been made in our understanding of the nucleus. A wealth of two-body scattering experiments have led to an accurate description of the nucleon-nucleon interaction. An even greater body of data is available on the properties of nuclear states, both from scattering experiments and from radioactive decay studies.[4] And yet the core of the problem, a fundamental theoretical description of the nucleus is lacking. The nucleus is a many-body system, as is the atom. The atomic case is, however, more tractable. Because the electrons are in a strong "external field"--the Coulomb field of the nucleus--interparticle interactions are small by comparison and can be treated by perturbation theory. Furthermore the electrons are relatively far apart, so only two-body interactions are important. Neither of these simplifications are present in the nuclear case. To circumvent the difficulty of direct attacks involving formulation and diagonalization of the nuclear Hamiltonian, several simplifying models have been proposed to explain various nuclear properties. A nuclear model is a set of assumptions concerning the nature of the nuclear Hamiltonian to be used as a basis for calculations. Experiments are performed to test the basic validity of these models. The comparison of other

properties with the model then shows how to modify the model if possible, to widen its field of application.

One much used model of the nucleus is the single particle or shell model. Its basis in experimental fact is identical to that of the atom; namely, that many properties of nuclei seem to undergo abrupt changes at certain values of both Z, the number of protons and N, the number of neutrons. Near these "magic" values the predictions of the extended shell model have become highly accurate and reliable.

The collective model on the other hand assumes that the nucleons act in concert and behave much like a liquid drop which vibrates and rotates. In fact, like a liquid drop, a nucleus can vibrate beyond the point that surface tension can act as restoring force and thereby split into two parts. Besides this process, called fission, many nuclei exhibit the energy spectra of a rotator or vibrator. Enhancement of electromagnetic transition probabilities and electromagnetic moments also support this model.

The nucleus is a system of spin 1/2 particles. Scattering of a nucleon from this system is called elastic if the nucleon suffers a change in only the direction of its momentum. To the extent that the nucleon-nucleon interaction can be represented by an average of two particle interactions, elastic scattering can be represented as scattering by an average single particle potential. This is called the optical model in analogy to the scattering of light. Elastic scattering is a direct process--it occurs roughly in the time it takes the incident nucleon to cross the nucleus. Other direct processes can occur with different initial and final states. For

example, an incident proton can excite a proton near the Fermi level above it and still have sufficient energy to scatter to an unbound state.[5] The cross section for this process can be calculated using the Born approximation, with the wave functions of relative motion of entrance and exit channels calculated using the optical model potential. It is also possible, however, that after the initial nuclear interaction the proton is in a bound state. No particle emerges immediately, and further collisions spread the excitation energy over the whole nucleus. This state is called the compound nucleus. It exists until random collisions give any one particle more energy than its binding energy, or until it decays by gamma-ray emission.

These are several of the models currently in use, each applicable to a particular aspect of the nucleus. Ultimately, the nuclear Hamiltonian will be derived from first principles, and each model will appear as an approximation to it. Until then it is desirable to test critical features of models, in order to understand how and how well each approaches reality. In this thesis two of these models will be tested.

The shell model was postulated because of the discovery of magic numbers. Near closed shells, its validity is greatest, and its description of nuclei simplest. Measurements of lifetimes in Nb^{92} and Nb^{94} which provide a sensitive test of the purity of shell model wave functions will be reported in this thesis.

The character of spin-zero excited states has provoked much interest of late. The 0' state in Kr^{80} should provide a test of the

vibrational nature of excited states of a "spherical nucleus" by the measurement of the probability for its decay by E0 radiation.

B.1. Shell Model

As long ago as 1933, an independent particle model of the nucleus was proposed, on the basis of systematic irregularities of nuclear properties.[6] For example, when the nucleus contains a "magic" number of protons and neutrons the binding energy per nucleon for that nucleus is large compared to the nuclei with one more or one less nucleon. Therefore the separation energy of the first nucleon from "magic number" plus-one nuclei is small. This suggests a shell structure, similar to the atomic case. If we assume non-interacting particles moving in an average potential generated by all the other particles, calculating the energy spectrum using a simple average potential such as the harmonic oscillator or a square-well, yields a series of levels, each having a high degeneracy. The difference between our model Hamiltonian and the actual nuclear interaction is called the "residual interaction." If the residual interaction is small compared to the average central potential, the splitting of the degenerate harmonic oscillator levels is small and the appearance is of large gaps in the eigenspectrum. Each group of levels between two gaps is a "shell." A nucleus having all the levels below a gap filled is called a closed shell nucleus. This number of nucleons (protons or neutrons) would be a magic number.*

*Although protons and neutrons are equivalent in the nuclear interaction, the Coulomb interaction causes the protons to fill the eigenstates at a slower rate than the neutrons, for nuclei of maximum stability.

However for all central potentials, the calculated magic numbers assume the wrong values. Independently Mayer[7] (using a suggestion of Fermi's), and Haxel, Jensen and Suess[8] proposed a Hamiltonian of a central potential plus a strong spin-orbit interaction.

A strong spin-orbit force splits each square-well level, with orbital angular momental ℓ, and degeneracy $4\ell + 2$, into levels $j_+ = \ell + \frac{1}{2}$, and $j_- = \ell - \frac{1}{2}$, each with degeneracy $2j + 1$. This eigenspectrum exhibits gaps between different levels than without the spin-orbit force, and yields the experimental magic numbers. This model successfully predicts the ground state spin in all even-even nuclei (zero) and in practically all odd-A nuclei, positing only the assumptions: one, pairs of nucleons in a given orbit tend to couple their angular momentum to zero; and two, the energy gained by particles pairing increases monotonically with j. This model, called by Preston[9] the "extreme single particle model," provides a set of basis states, for further refinement of the predictions.

It must be noted that the success of such a simple model, in which independent nucleons move in an average potential is deceptive. The assumptions mentioned above imply that there exists very strong pairing force, at least between nucleons of the same orbital angular momentum. This pairing is also implied by the empirical fact of the superior stability of even-even nuclei. The existence of deformed nuclei and data on the enhancement of electromagnetic moments and transition rates indicate that long-range multiple-particle correlations play an important role in the nuclear Hamiltonian.

B.2. Effective Interaction

One method of improving on the extreme single particle model is to use the fact that near magic numbers, shell effects are greatest. Therefore the nucleus can be considered to be a magic number of nucleons plus several valence nucleons, in the hope that low lying states will be due to residual interactions among the valence particles, the interaction with the core being constant.[10,11] If we further assume that only two-body interactions between valence nucleons are important, our nuclear Hamiltonian is given by

$$H = H_{\text{core}} + \sum_{\text{nucleons}} H_{\text{core-valence nucleon}} + \sum_{\substack{\text{nucleon} \\ \text{pairs}}} H_{ij}$$

Our assumptions are then that the valence nucleons do not interact with the inert core.

$$|\text{nucleus}\rangle \equiv |\alpha, Z, N\rangle = |\text{core}\rangle|\text{valence nucleons}\rangle \equiv |Z_c N_c\rangle |I = Z - Z_c, K = N - N_c\rangle$$

where α is a serial number of excited states.

$\langle \alpha', Z, N | H_{\text{core}} | \alpha Z N \rangle$ = constant; for low-lying states

$\langle \alpha', Z, N | H_{\text{core-valence nucleon}} | \alpha Z N \rangle$ = constant; for low-lying states

We further assume that our i-proton, k-neutron basis states are eigenstates of ΣH_{pp} and ΣH_{nn}.

$$\sum_{\substack{\text{valence}\\ \text{pairs}}} H_{ij} = \sum_{\substack{\text{protons}\\ \text{pairs}}} H_{pp} + \sum_{\substack{\text{neutron}\\ \text{pairs}}} H_{nn} + \sum H_{pn}$$

$$|\alpha,i,k,I\rangle = |[\alpha_p,(j_p)^i\, J_p,\alpha_n,(j_n)^k\, J_n]I\rangle$$

$$= |[J_p,\alpha_p,J_n,\alpha_n]I\rangle$$

where I is the total nuclear angular momentum, and α_p and α_n are serial numbers for various couplings to the same J. We then diagonalize the Hamiltonian (energy matrix) in this representation for each value of I

$$E(J_p',\alpha_p',J_n',\alpha_n';J_p,\alpha_p,J_n,\alpha_n) = \langle[J_p',\alpha_p',J_n',\alpha_n']I|\sum_{\text{pairs}} H_{ij}|[J_p,\alpha_p,J_n,\alpha_n]I\rangle$$

$$= F_p(J_p,\alpha_p)\delta_{[\ ]} + E_n(J_n,\alpha_n)\delta_{[\ ]}$$

$$+ iKE_{pn}(J_p',\alpha_p',J_n',\alpha_n';J_p,\alpha_p,J_n,\alpha_n;I)$$

where

$$\delta_{[\ ]} = \delta_{J_p'J_p}\,\delta_{\alpha_p'\alpha_p}\,\delta_{J_n'J_n}\,\delta_{\alpha_n'\alpha_n}$$

E_p, E_n and E_{pn} are obtained from the B^I_{pp}, B^I_{nn}, B^I_{pn}, the two particles matrix elements

$$B^I_{pp} = \langle(j_p')^2_I|H_{pp}|(j_p)^2_I\rangle$$

$$B^I_{nn} = \langle(j_n')^2_I|H_{nn}|(j_n)^2_I\rangle$$

$$B^I_{pn} = \langle(j_p',j_n')_I|H_{pn}|(j_p,j_n)_I\rangle$$

These may be calculated using assumed residual potentials, or may be obtained from experimental level schemes of nuclei having

respectively 2 protons; 2 neutrons; and, 1 proton and 1 neutron outside of the core. In either case, the diagonalization yields the energy spectrum, and the amplitudes of each wave function in the basis representation. These wave functions may be used to calculate electromagnetic transition probabilities, and stripping and pickup reaction cross sections.

This method has been applied most vigorously to the region near A = 90. There is a shell closure at N = 50 and minor shell closures at Z = 38, $_{38}Sr^{88}_{50}$, and at Z = 40, $_{40}Zr^{90}_{50}$. One of the more interesting nuclei in this region is $_{41}Nb^{92}_{51}$. Considering Zr^{90} as the inert core, the low-lying states should be the result of the interaction of a single proton with a single neutron. With Sr^{88} as the core, the single neutron interacts with three protons. In Figure 1 is shown a comparison of the low-lying states in Nb^{92} as determined both experimentally and theoretically. Ball[12] has calculated these levels using a Sr^{88} core, the neutron being in the $2d_{5/2}$ orbital and the three protons in the $2p_{1/2}$ and $1g_{9/2}$ orbitals. Vervier[11] and Auerbach and Talmi[13] have used a Zr^{90} core and considered only the single $g_{9/2}$ proton and single $d_{5/2}$ neutron or in standard notation, the wave function is written as $\pi g_{9/2}\,\nu d_{5/2}$. All three performed a least-squares fit to all the data available and then recalculated the Nb^{92} spectrum. The deviations of the recalculated spectra from the experimental spectrum is an indication of the accuracy of the calculations. The six spectra to the right of the experimental spectrum in Fig. 1 were all calculated using theoretical matrix elements of harmonic oscillator wave functions. Pandya[14] couples

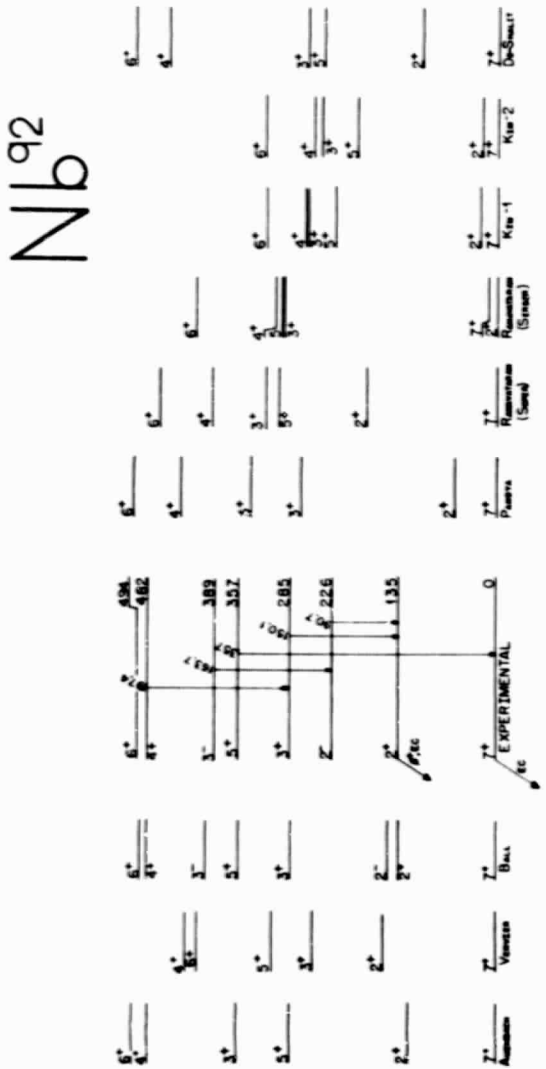

Fig. 1. Comparison of Experimentally Measured and Theoretically Predicted Low-Lying States in Nb^{92}.

a $1g_{9/2}$ proton and a $2d_{5/2}$ neutron outside the Zr^{90} core, using a mixture of Wigner and Majorana (spin-exchange) potentials. The radial dependence of the potentials is Gaussian. De-Shalit's[15,18] calculation is identical except that a zero-range force is used. Ramavataram's "Serber" calculation is the same as Pandya except that; first, the ratio of strengths of Wigner and Majorana potentials is changed; second, the neutron, in either the $2d_{5/2}$ or $3s_{1/2}$ states is coupled to the ground state of Nb^{91} which is given by the "experimental" configuration

$$83\% \ (2p_{1/2}^2 \ 1g_{9/2}) + 17\% \ (1g_{9/2}^3);$$

third, whereas, Pandya and De-Shalit normalize the absolute strength of the interaction to fit the $7^+ - 6^+$ splitting, Ramavataram uses the value that gave the best fit to Y^{90} experimental spectrum. In his "Soper" calculation, Ramavataram uses a mixture of spin and exchange forces.*

Kim's results are calculations of the levels of Y^{90}. He uses a Sr^{88} core and places the odd proton and neutron in the $1g_{9/2}$ or $2p_{1/2}$, and $2d_{5/2}$, $3s_{1/2}$, $2d_{3/2}$, or $1g_{7/2}$ levels, respectively. His interaction is a combination of central and tensor potentials. Because his computed wave functions show very little configuration mixing, we can use his results for the $\pi g_{9/2}\ \nu d_{5/2}$ spectrum outside

---

*Formally, a combination of Wigner (no exchange), Bartlett (spin exchange), Heisenberg (spin and space exchange), and Majorana (space exchange) forces. This is the most general central potential that can be written. c.f. Preston, pp. 16-17.

a Zr^{90} core. Kim also predicts the negative parity spectrum. However, because they are the spectrum of $\pi p_{1/2} \nu d_{5/2}$, the ground state of Zr^{90}, which is mainly $\pi p^2_{1/2}$ cannot be used as a core. His prediction for the relative spacing of the two negative parity levels is 35 keV and 29 keV, respectively.

It can thus be seen that reasonable accuracy in predicting energy levels can be achieved with this method provided the interaction matrix elements can be obtained. The calculated wave functions can be used to further test this theory by predicting reaction cross sections and electromagnetic transition probabilities. Sheline et al.,[18] Sweet et al.,[19] and Ball and Cates[20] have observed the Nb^{92} states via pickup and stripping reactions. The relative cross sections agree very well with theoretical values obtained using the wave functions of Ball. It is interesting to note that their results do not yield a unique set of spin assignments since the model predicts no significant difference in the cross sections of the 28[illegible] and 355 keV states if their assigned spins are interchanged.

The same configurations that dominate the low-lying states in Nb^{92} should be present in Nb^{94}. They differ only by the addition of two $d^2_{5/2}$ neutrons, which the simple shell model predicts should couple to zero. An extensive decay scheme for Nb^{94} has been deduced by Jurney et al.[23] from studies of stripping and neutron capture on Nb^{93}. They have calculated the $Nb^{93}(d,p)Nb^{94}$ cross sections and find them in fair agreement with the data of Sheline et al.[22] Their calculations of relative M1 transition probabilities is in fair

agreement with the data of Gruber et al.,[21] who have measured the gamma rays following neutron capture by Nb^{93} with a bent crystal spectrometer. No attempt has been made to calculate the electromagnetic dipole (E1) transition probability for the E1 transitions in both nuclei. We do know, however, that in Nb^{92} the negative parity states should result from the coupling of a $d_{5/2}$ neutron to a proton configuration $p_{1/2}\, g^2_{9/2}$, assuming a Sr^{88} core. The positive parity states are explained by the coupling of the neutron to a $g^3_{9/2} + g_{9/2}\, p^2_{1/2}$ configuration. The same may be said for Nb^{94} except that the neutron configuration is $d^3_{5/2}$. The E1 transition corresponds therefore to the transition of a proton from $p_{1/2}$ to $g_{9/2}$, or from $g_{9/2}$ to $p_{1/2}$. This implies a change in total angular momentum of 4. Therefore, in this approximation, this transition is forbidden. Table 1 shows the single particle estimates for these transitions, assuming a parity change. A strict shell model interpretation implies only E3 transitions with half-lives of the order of a second for both gamma rays.[24] A more realistic statement is that the half-life is long compared to the E1 estimate and is a measure of the mixing of other configurations into the simple ones.

C.1. Even-Even Nuclei

A survey of the systematics of the low-lying states of even-even nuclei reveals certain striking patterns.[25,26,27] Without exception the spin of their ground states is zero, even parity.[27] This is explained in the shell model assumptions as due to pairing forces, so

Table 1. Weisskopf Estimates of Half-Lives of Transitions in Nb^{92} and Nb^{94}

Multipolarity	Gamma Ray	Nb^{92} E_γ = 90 keV Internal Conversion	Total
E1	.31 ps	1.7 ps	.26 ps
M2	5.0 μs	1.3 μs	1.0 μs
E3	16 s	.70 s	.67 s
M4	1.4 Gs	2.7 Ms	2.7 Ms

Multipolarity	Gamma Ray	Nb^{94} E_γ = 100 keV Internal Conversion	Total
E1	.22 ps	2.0 ps	.20 ps
M2	2.8 μs	1.3 μs	.88 μs
E3	7.1 s	.71 s	.64 s
M4	.53 Gs	2.0 Ms	2.0 Ms

Note: 1 year = 31.56 Ms

1 month = 30 days = 2.59 Ms

that the lowest energy state has all nucleons coupled to zero total angular momentum.[25] Secondly, with few exceptions, the first excited state of these nuclei has spin 2, even parity.[26] In the region of nuclides with masses $50 < A < 150$, this state lies about 0.5 to 1.5 MeV above the ground state. The second excited state usually lies another 0.5 to 1.5 MeV above the first excited state. The most common spins and parities are 0^+, 2^+, or 4^+. Another striking trend is the large values for the reduced electric quadrupole transition probabilities, B(E2). They are one order of magnitude greater than those calculated using the assumption that a single particle deexcites from one shell model orbit to another. This suggests the motion of particles in concert. The simplest model that shows these characteristics is a vibrating liquid drop. The relative incompressibility of nuclear matter precludes a monopole or "breathing" mode. Since dipole motion corresponds to displacement about the center of mass, the lowest available vibration is quadrupole in shape. This yields a set of degenerate states at excitation energies $\hbar\omega_2$, $2\hbar\omega_2$, $3\hbar\omega_2$, ... above the 0^+ ground state, as can be seen in Figure 2. Also shown are higher order shape oscillations--octupole and hexadecapole vibrational states. The octupole states have been observed experimentally to lie at excitation energies of one to three MeV; evidence for the hexadecapole state is still inconclusive.

Note also that in the "pure vibrator" model the three two-phonon states are degenerate, whereas in real nuclei they are separated by

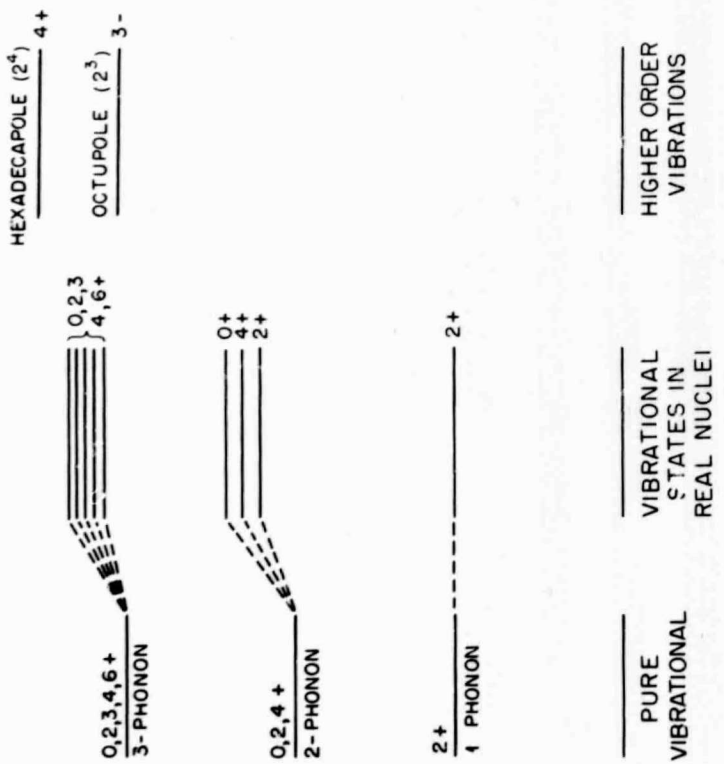

Fig. 2. Comparison of Schematic Experimental and Theoretical Spectra for a Typical Spherical Even-Even Nucleus.

as much as a few hundred kilovolts. One method to remove the degeneracy is to consider an anharmonic vibrator. For example, Kerman and Shakin[28] have done this by including the cubic term in their Hamiltonian, but find their results are valid only for the case that the ratio of the excitation energies of the members of the "two-phonon" triplet to the first 2^+ state is less than 2. This condition unfortunately does not hold for all nuclei in this region. In fact, as Mitra and Pal[29] have shown, there is no reason to add only cubic terms. The cubic approximation will work only in those cases where higher order terms cancel or are small.

C.2. The Vibrator

Several authors[30,31,32] have performed calculations of the properties of the vibrational mode. Reiner[30] started from a simple harmonic Hamiltonian

$$H = \sum_{\mu=-2}^{2} \frac{|\pi_\mu|^2}{2B} + \frac{B\omega^2}{2} |\alpha_\mu|^2$$

where α_μ is the quadrupole deformation, and π_μ its conjugate momentum. Introducing the operators,

$$\alpha_\mu = \sqrt{\frac{\hbar}{2B\omega}} (b_\mu + (-1)^\mu b^+_{-\mu})$$

$$\pi_\mu = i\sqrt{\frac{\hbar B\omega}{2}} (b^+_\mu - (-1)^\mu b_{-\mu})$$

transforms the Hamiltonian to

$$H = \hbar\omega \left(\frac{1}{2} + \sum_\mu (-1)^\mu b^+_{-\mu} b_\mu\right)$$

The eigenspectrum of this Hamiltonian is

$$|0>,$$

$$b_\mu^+|0>,$$

$$\frac{1}{2}\sum_m \begin{pmatrix} 2 & 2 & I \\ m & M-m & -M \end{pmatrix} b_m^+ b_{M-m}^+ 0>, \ldots.$$

This then allows one to calculate transition probabilities.* For example from Bohr and Mottelson[33] the B(E2) is given by

$$B(E2) = \left(\frac{5}{4\pi} Z<r^2>\right)^2 \sum_{\mu,M_f} |<I_f M_f|\alpha_\mu^+|I_i M_i>|^2$$

Thus is it simple to calculate

$$B(E2, 0_0^+ \to 2_1^+) = \left(\frac{5}{4\pi} Z<r^2>\right)^2 \frac{5\hbar}{2B\omega}$$

$$B(E2, 2_2^+ \to 0_0^+) = 0$$

$$B(E2, 0_2^+ \to 2_1^+) = B(E2, 2_2^+ \to 2_1^+) = B(E2, 4_2^+ \to 2_1^+) = \left(\frac{5}{4\pi} Z<r^2>\right)^2 \frac{\hbar}{B\omega}$$

These formulae can then be compared with experimental results. B(E2) values are usually measured via Coulomb excitation. The Oak

*It should be noted that Reiner's state vectors are not normalized. If the n-phonon state of spin I, magnetic quantum number is n,I, μ, then his state vectors yield

$$<0,0,0|0,0,0> = 1$$

$$<1,2,\mu|1,2,\nu> = \delta_{\mu\nu}$$

$$<2,I,\mu|2,I,\nu> = \frac{1}{4I+2}\delta_{\mu\nu}$$

Ridge group has made systematic measurements of ruthenium,[35] palladium,[34] and cadmium[36] even-even nuclei.

They find in all the nuclei that the B(E2; $2_1^+ \to 0_0^+$) is enhanced by a factor of 20 to 60 over single particle estimates. The selection rule on the 2_2^+ to 0_0^+ transition is weakly violated: all of these transitions have single particle B(E2)'s. The ratio B(E2; $J_2^+ \to 2_1^+$)/ B(E2; $2_1^+ \to 0_0^+$) is predicted by the phonon model to be 2. If J is 4 this ratio is measured to be between 1 and 2; if J is 2, between 0.5 and 1.5; if J is 0, between 0.5 and 1.0. Thus these transitions are enhanced, but not as much as the phonon model would predict. The phonon model also fails to account for the large quadrupole moments of the 2_1^+ states.[37,38,39] This may however also be accounted for by anharmonic effects.[40]

Thus tests derived from electromagnetic quadrupole matrix elements are inconclusive. There are other tests of the theory. Reiner[30,41,42] has calculated the probability, W(E0) for the decay of the 0_2^+ state, by electron conversion, to the ground state 0_0^+.

$$W(E0) = B(Z)F(Z,E,R_o)|M_{fi}|^2$$

where

Z is the atomic number

R_o is the nuclear radius = 1.2 $A^{1/3}$ Fermi

B(Z) is a function of the model of the atomic electron distribution used

F is a function similar to the Fermi function

E is the E0 transition energy

The factor $|M_{fi}|^2$ represents the nuclear effect on the transition probability. This is calculated using the proper state vectors and the E0 transition operator, which is proportional to

$$\beta^2 = \sum_{\mu} |\alpha_{\mu}|^2 ,$$

$$= \frac{\hbar}{2B\omega} \sum_{\nu} [b_{\nu}b_{\nu}^{+} + b_{-\nu}^{+}b_{-\nu} + (-1)^{\nu} b_{\nu}b_{-\nu} + (-1)^{\nu} b_{-\nu}^{+}b_{\nu}^{+}]$$

Inspection of this equation and of the definition of B(E2) reveal an important difference between the two. The B(E2) operator is linear in the b's and therefore only connects states whose phonon numbers differ by one. The E0 operator is quadratic in the b's and therefore only connects states whose phonon numbers differ by two. Reiner expresses his result as the ratio of the number of E0 electrons to the number of E2 photons resulting from the decay of the 0_2^+ state.

$$\mu_k = \frac{W^{E0}(k, 0_2^+ \rightarrow 0_0^+)}{W^{E2}(k_\gamma, 0_2^+ \rightarrow 2_1^+)}$$

$$= \frac{375}{8\pi\alpha} B(Z)\, F_k(Z,k,R_o)\, k_\gamma^{-5}\, \frac{\hbar}{B\omega}$$

where $\hbar = m_e = c = 1$

$\alpha = \frac{e^2}{\hbar c} = .0072972$ is the fine structure constant

k_γ is the E2 transition energy

k is the E0 transition energy

With a view to testing this equation let us consider the decay scheme of Br^{80} in Figure 3.[45] Although all members of the two-phonon triplet

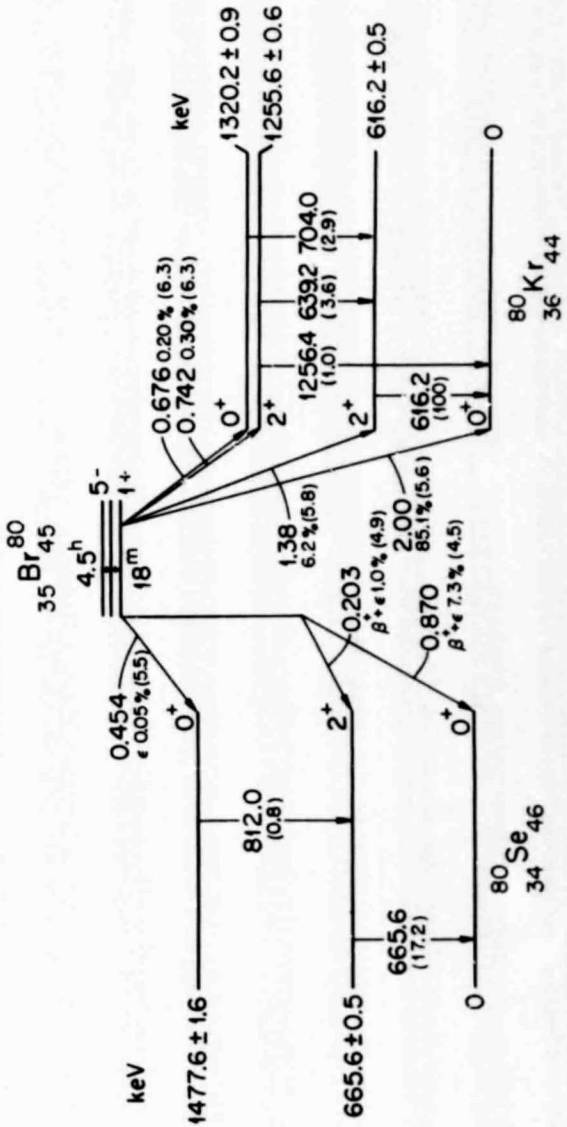

Fig. 3. Decay Scheme of Br^{80} (from Ref. 45).

in either Se^{80} or Kr^{80} are not yet known, there is good evidence that the states shown are phonon states. Heydenburg et al.[43] have measured the relative B(E2)'s for the first excited state of all krypton nuclei. Using Beard's[44] value for the $B(E2, 2_1^+ \rightarrow 0_0^+)$ in Kr^{82}, we find

$$B(E2, 0_0^+ \rightarrow 2_1^+) = .39\ e^2 \times 10^{-48}\ cm^4$$

for Kr^{80}. This represents an enhancement factor of 36 over the Weisskopf estimate. For Se^{80} this factor[46] is 26. The decay of the 1255 keV level in Kr^{80} shows that the enhancement of the cascade to crossover is 97, showing the weakness of the forbidden crossover.[45] This nucleus therefore is very close to the vibrator and a measure of the decay of the 0_2^+ state by a monopole transition may provide another test of this model. Using Reiner's formulae we expect μ_k to be 3.6×10^{-4} for Kr^{80}, 1.2×10^{-4} for Se^{80}. If this weak transition can be detected, it should provide a sensitive test of the phonon model.

CHAPTER II

A. Equipment

To measure the properties to be tested required many of the tools of gamma ray and electron spectroscopy. Both experiments, as shall be seen later, demanded the detection of gamma rays or electrons. Also necessary was the manipulation of electronic signals from the detectors.

To detect gamma rays a lithium-drifted germanium detector, Ge(Li), was used. Typical energy resolution of 3.5 keV full width at half-maximum (FWHM) was obtained for gamma ray energy ≈ 150 keV with the 30 cc detector used for the lifetime measurements. Because the carrier mobilities in germanium are small compared to the speed of light, the time taken to collect the charge is long and it is difficult to do excellent timing with these detectors. For example, the inset in Figure 4 shows the prompt timing curve from the Rb^{94} measurement. The slope of the left side is near ten nanoseconds. The slope of the right side, which shows the contribution due the beam-pickoff, is, by comparison, less than two nanoseconds. The width of the prompt peak is narrow because the dynamic range* of pulses used was restricted to less than two.

---

*The ratio in one channel of the maximum pulse height to the minimum pulse height.

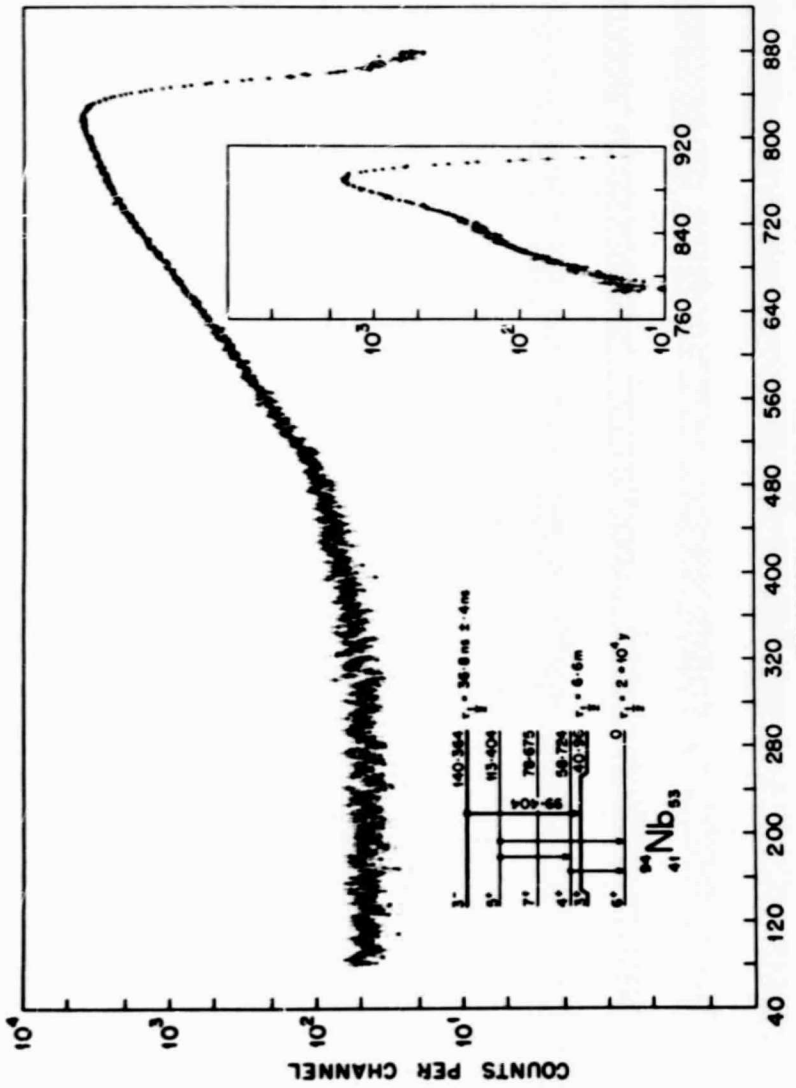

Fig. 4. The Decay of the 99.404 keV Gamma Ray from the Reaction $Zr^{94}(p,n)Nb^{94}$; (right inset) Prompt Peak; (left inset) Level Scheme of Nb^{94}.

To detect conversion electrons and beta rays, two detectors were used. One was a lithium-drifted silicon detector Si(Li); the other, a plastic scintillator optically coupled to a photomultiplier. The silicon detector was a planar type with about a 1.5 cm^2 cross section and a 4 mm active depth.* Because of its poor room temperature noise characteristics, it had to be operated at liquid nitrogen temperature. Initially its resolution was nine keV for the 975 keV line in Bi^{207}, but this broadened to 20 keV during the course of the experiment.

The other detector was a 2.5 cm by 2.5 cm cylinder of NE 102 plastic scintillator, coated with titanium dioxide to improve reflectivity. It was optically coupled by opthamalogical grease to the face of an RCA 8575 photomultiplier, chosen for its low noise characteristics. The NE 102 system had an energy resolution $\Delta E/E$, of 13% for the 975 keV electron line in Bi^{207}. Figure 5 shows the timing curve of the Si(Li)-plastic coincidence system found using a Bi^{207} source. Each of the detectors produces an electronic signal containing information on the energy and arrival time of the detected radiation. For the solid state detectors the energy is proportional to the number of hole-electron pairs produced by ionization. A charge-sensitive preamplifier produces an output pulse whose height (voltage) is proportional to the input charge.

To obtain the energy of the radiation the height of the output pulse from the preamp is measured usually with a multichannel

---

*This detector was fabricated by Dr. K. J. Casper and by H. M. Trammel.

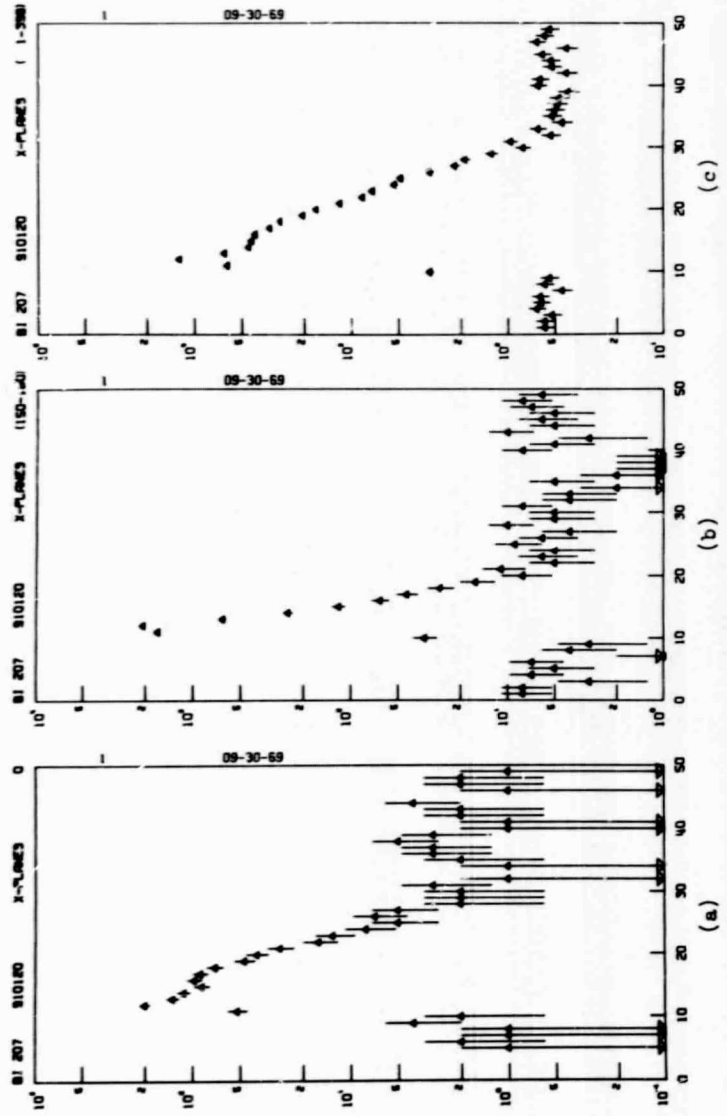

Fig. 5. Coincidence Delay Curves of Bi^{207} Using a Si(Li)-Plastic Scintillator System; (a) All Coincidences, Singles; (b) Only 975 keV line in Si(Li); (c) All Coincidences, Sum of Coincidence Matrix Energy Planes.

analyzer (MCA). This device stores an input pulse (a count) in a numbered bin (channel) whose number is proportional to height. A single-dimensional analyzer was used for the gamma-ray studies. A two-dimensional analyzer was used for the electron-electron coincidence work. This instrument accepts two pulse inputs and has two modes of operation. One accepts and counts pulses from either input (called X and Y) and stores them as a single-dimensional analyzer. In the other mode, the MCA stores coincident pulses from X and Y, in a matrix whose row and column numbers are the channel numbers of the X and Y input respectively. To obtain time information a time-pickoff (TPO) was used.* This device emits an output pulse whenever any input pulse rises above a certain adjustable "bias level." This method is known as "leading edge triggering." The time between two pulses can be determined using a time-to-amplitude converter (TAC) which emits a pulse whose height is proportional to the difference in the arrival times of two input pulses. Because of internal electronic requirements the lower rate pulse is used to START, and the higher rate pulse to STOP the TAC.

The spectrum of output pulses may be displayed on an MCA. Other devices needed are: A single channel analyzer (SCA) produces an output pulse whenever an input pulse has a height which falls between two adjustable limits. A linear gate (LG) emits an output pulse upon receiving an input pulse, if and only if it has been

---

*All logic generating electronics were obtained from ORTEC, Inc.

previously opened (enabled, "gated") by a second ("gate") pulse. A gate generator (GDG) creates pulses with proper shapes to enable an LG. A shaping amplifier (SA) is an active high and low pass filter used to present the MCA with a pulse shape it prefers.

The last piece of equipment to be mentioned is the Van de Graaff accelerator. A pulsed proton beam from the 6 MeV Van de Graaff used to populate the excited states of the niobium isotopes. It is desirable that the width of the pulses, Δx in distance, or $\Delta t = \Delta x/v$ in time, where v is the velocity of the ions, be as small as possible. This is accomplished by chopping the output of the ion source and bunching the pulses before they are accelerated. The resultant pulse can have a width as small as a nanosecond, and a repetition rate variable in steps of factors of two from an eight to two megahertz.[47,48] The arrival of the beam pulse is announced by detection of charge induced on a capacitor (BPO) through which the beam passes. This device is similar to a TPO in operation.

Having introduced the tools used, it is time to proceed to indicate how they were used.

B. Experimental Details of Zr(p,n)Nb Experiments

B.1. Philosophy

As was discussed in section I. B. 2, several groups have studied the levels in Nb^{92} and Nb^{94}. Each method that was used, highlights different aspects of these level schemes. The pickup reaction $Nb^{93}(d,t)Nb^{92}$, for example, is very specific; it populates only the six states corresponding to $\pi g_{9/2}{}^{\nu}d_{5/2}$. The capture reaction leading

to the excited states is quite the opposite. Although the spins of possible capture states are only 4 or 5, gamma cascades from all of the low lying levels exist. What then are the features of the $(p,n\gamma)$ reaction and why was it used?

At the low bombarding energies used (2-6 MeV), the (p,n) reaction proceeds via the compound nucleus. Thus, unlike the pickup and stripping reactions, the relative populations of final states are independent of the configuration of the target nucleus. Cross sections may be calculated using the "statistical model."[49] The most important influence on the cross sections are by the "angular momentum barrier," as we shall see later.[50]

Unlike the capture process, (p,n) is an endothermic reaction. and involves the influx of a charged particle. Thus the population of each level of the final nucleus has a sharp threshold as a function of bombarding energy. This affords us three advantages. First by measuring the threshold of each gamma ray from the $(p,n\gamma)$ reaction we know its exact placement in the level scheme. Secondly, if we take gamma spectra at low bombarding energies we have fewer gamma rays to contend with and data analysis is considerably more straight forward. Thirdly, since the (p,n) reaction can be performed using a pulsed accelerator, states with lifetimes greater than 10^{-9} seconds can be identified and their half-lives measured.

These facets of the (p,n) reaction are illustrated in Figures 6 and 7. They show spectra of gamma rays following the indicated (p,n) reactions, for successively higher bombarding energies. Note,

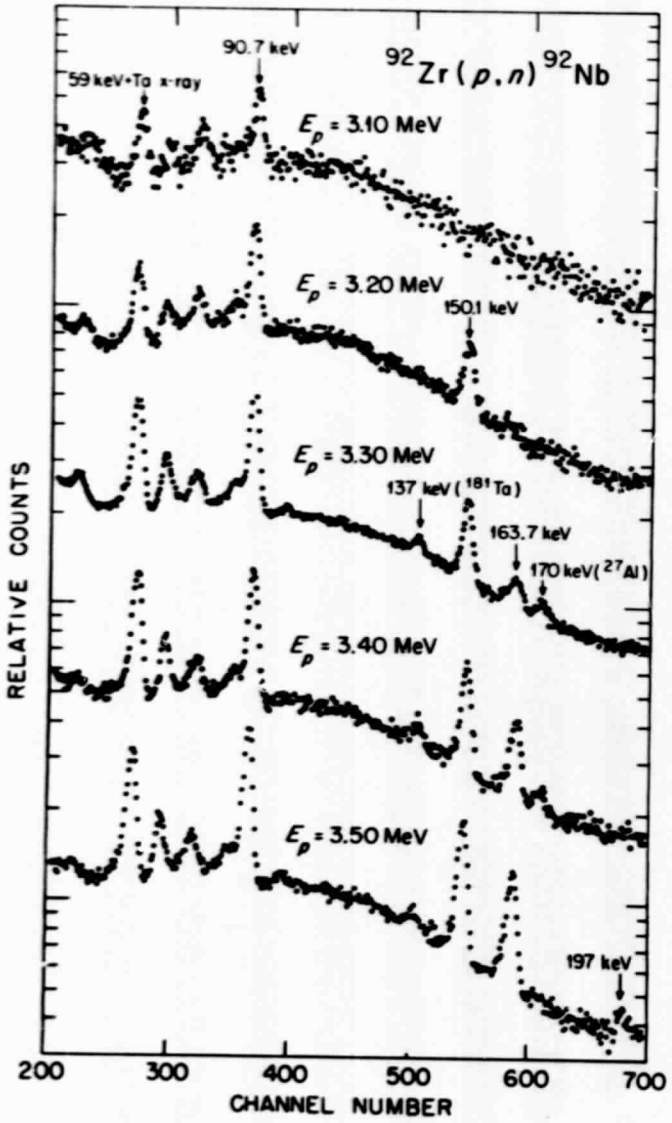

Fig. 6. Energy Spectra of Gamma Rays Following the $Zr^{92}(p,n)Nb^{92}$ Reaction.

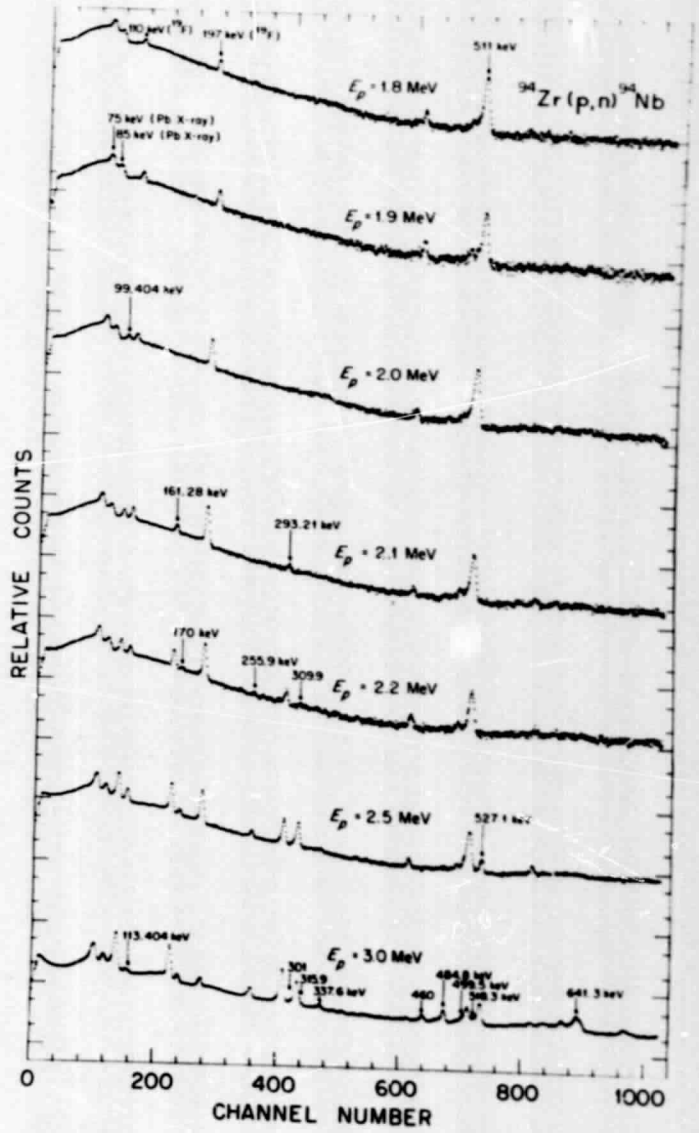

Fig. 7. Energy Spectra of Gamma Rays Following the $Zr^{94}(p,n)Nb^{94}$ Reaction.

for example, the sharp threshold of the 163.7 keV gamma ray in the Nb^{92} spectra at about 3.25 MeV. This gamma ray depopulates the 3^- state at 389 keV in Nb^{92}.

Also present are the thresholds of 90.7 gamma at less than 3.1 MeV; the 150.1 gamma, at 3.15 MeV; and the 197 keV gamma, at 3.5 MeV. It must be noted that the continuing increase in all the peaks attributable to Nb^{92} is due, not to increasing excitation of the decaying level, but to population of lower states by gamma ray cascade from higher directly populated states.

The peaks labeled as X-rays are the result of protons, elastically scattered from the target, causing the lining of the scattering chamber to fluoresce. These cross sections have been recently shown to be quite large, accounting for the size of the peaks.[51] The peaks attributed to Ta^{181} and Al^{27} are the result of inelastic scattering of protons or neutrons from parts of the inside of the scattering chamber. The peaks attributed to F^{19} are the result of inelastic scattering from impurities in the target.* All of these peaks can be distinguished from (p,nγ) peaks by the simple fact that none are produced by reactions that have sharp thresholds.

In the Nb^{94} spectra, compare the number of gamma rays in the 1.8 MeV spectrum (.1 MeV above the ground state threshold) with the

*This was verified in an amusing way. During one of the Nb^{94} runs the ion source of the Van de Graaf malfunctioned. As a result, the beam intensity wandered to a very high value, burning a hole in the target. Gone was the discoloration spot which had accumulated during the course of many experiments. When the target was remounted, using a fresh portion of the target, the F^{19} lines were much less intense than before.

number in the 3.0 MeV spectrum (1.3 MeV above the ground state threshold), noting that the energy scale covers only 0-800 keV. In the latter spectrum data analysis is practically impossible. Gamma ray energies were assigned using the values from the bent crystal spectrometer work of Gruber, et al. who studied the Nb^{93} capture gamma rays.

The effect of the angular momentum of the final state spin may be seen by comparing the rate of increase with increasing energy, of the 161 keV, 293 keV, and 256 keV gamma rays. They depopulate states in Nb^{94} at 301.4 keV, 333.9 keV, and 314.6 keV respectively. The spins of the respective states are 3^-, 2^+, and 5^+. It is obvious that the 5^+ state has a much smaller cross section than the low spin states. This is a result of the "angular momentum barrier." Although the out-going neutron has no Coulomb barrier to penetrate, the effect of the angular momentum is to add a repulsive term to the "effective potential."[52]

The pulsed beam from a Van de Graaff accelerator is ideal for populating short-lived isomers.[53] The beam pulse establishes a very accurate time scale. The detection of the decay of the isomer and the measurement of its lifetime is straight-forwardly accomplished using the tools described in Section II. A.

But the real importance of (p,n) in this experiment arises from the fact Nb^{92} and Nb^{94} are odd-odd nuclei. Because there is a paucity of stable odd-odd nuclei (5)* and an abundance of even-even

*$_1H^2_1$, $_3Li^6_3$, $_5B^{10}_5$, $_7N^{14}_7$, $_{73}Ta^{180}_{107}$.

nuclei (156), the charge exchange reaction is an obvious method to study the former using the latter as targets. This is a necessity, not a luxury, for many odd-odd nuclei have either no radioactive parent (e.g. Nb^{92} and Nb^{94}), an extremely short lived parent (e.g. Co^{38}-K^{38}), or the decay of the parent is not useful. An example of the latter is Ru^{94}-Tc^{94}. The beta decay of ${}_{44}Ru^{94}_{50}$ reveals only three states in Tc^{94} in the first MeV of excitation energy;[54] $Mo^{94}(p,n\gamma)Tc^{94}$ reveals eleven.[55]

B.2. Experiment

A schematic of the physical layout for the niobium isomer lifetime measurement is shown in Figure 8. A pulsed beam of protons from a Van de Graaffaccelerator (not shown) impinges on the target from the left. The arrival of the pulsed beam was sensed by the capacitive device (BPO) three meters before the target chamber. The chamber itself is aluminum and was lined with thin lead foil to minimize the gamma ray background resulting from the interaction of protons, elastically scattered from the target, with the walls of the chamber. The self-supporting foil target[56] was rolled from isotopically enriched zirconium metal. It was mounted vertically in a lead-faced aluminum target holder in the center of the chamber, at an angle of 45° to the incoming beam. Those protons, which passed through the target were stopped in the Faraday cup, which was a 17.8 cm diameter magnesium pipe, 3.05 m long. The flange at the far end contained a carbon block insert. This pipe was mated to the scattering chamber, through a gate valve by a piece of lead-lined steel

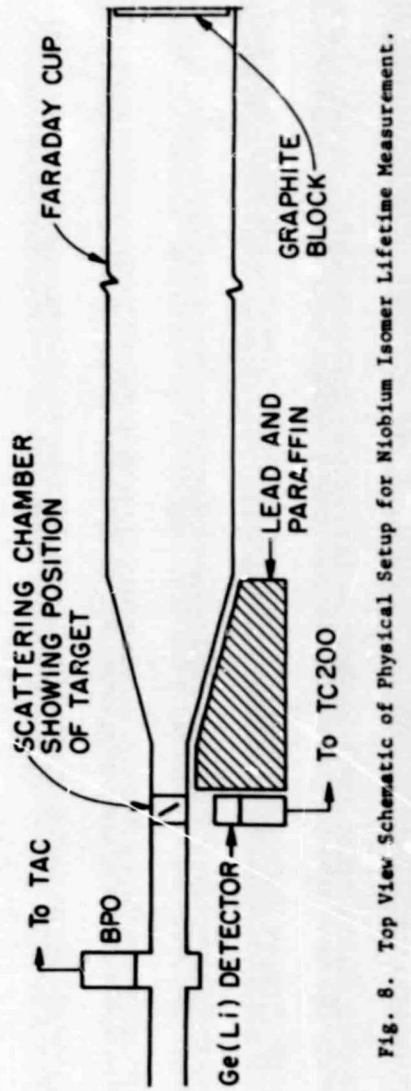

Fig. 8. Top View Schematic of Physical Setup for Niobium Isomer Lifetime Measurement.

pipe having about a 9.5° taper, to reduce background. In a previous attempt to measure these lifetimes, a pipe of smaller diameter was used beyond the target chamber. The time spectra showed several peaks corresponding to times after the arrival of the beam at the target. One source of these peaks was gamma rays from protons which had undergone multiple scattering in the target. This effect was calculated using the tables of Bichsel.[57] For 6 MeV protons incident on a one mg/cm^2 target of zirconium (Z = 40), 67% of all particles have trajectories which fell in a cone of half-angle .57°. For 1.5 MeV protons this is 2.8°. The pipe is such that only particles outside a cone of a half-angle of 7° will strike the tapered section. There is sufficient lead between the Ge(Li) detector and the magnesium pipe to attenuate gamma radiation from this source. Besides lead, paraffin was also used to attenuate any neutrons scattered back from the Faraday cup.

The detector viewed the target at 90° to the beam through a thin window in the chamber. For singles measurements its efficiency was calibrated by placing radioactive sources in place of the target.

Two typical electronic block diagrams are shown in Figures 9 and 10. The configuration in the latter was used to search for isomers. The arrival of the beam at the BPO is used to announce the creation of an excited state of the reaction product, by stopping the TAC. By use of delay line this occurs after the decay of the excited state is announced by the detection in the Ge(Li) detector of the product gamma radiation. The TPO pulse start the TAC. The

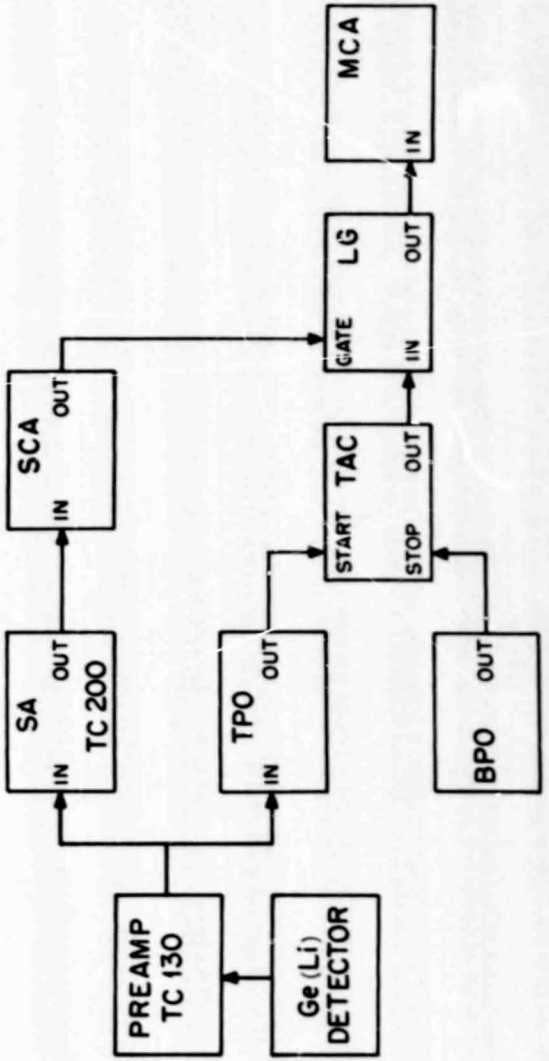

Fig. 9. Schematic of Electronic Setup for Niobium Isomer Lifetime Measurement.

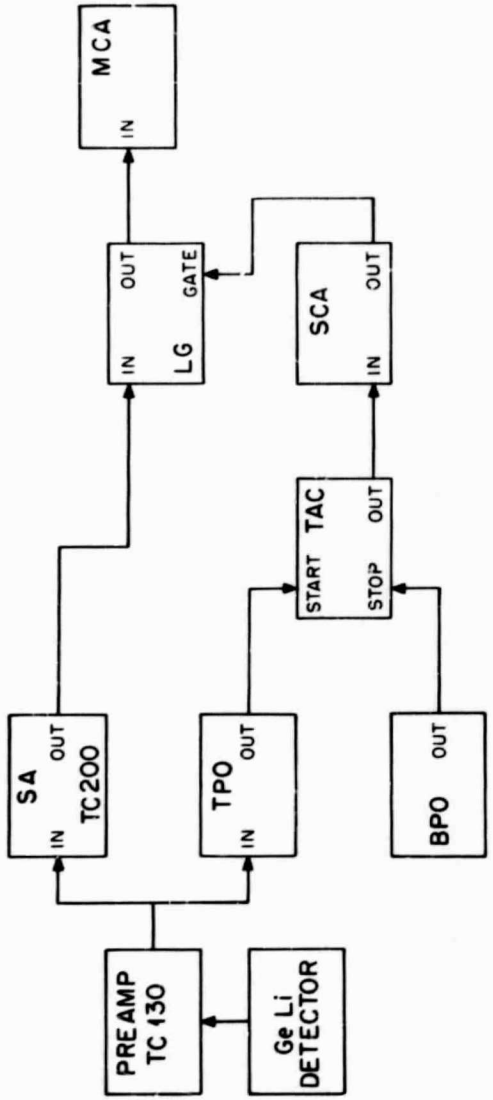

Fig. 10. Schematic of Electronic Setup for Niobium Isomer Search.

output pulse from the TAC enters the SCA, which is set to emit an output pulse only if the input pulse is in the center of the prompt peak ("gating on the prompt peak"), i.e. only if the gamma ray entered the Ge(Li) detector immediately after the target was irradiated. The SCA output pulse opens the linear gate (LG). Thus this gamma ray energy spectrum from the TC200 is filtered so that any gamma ray from the decay of a state, long-lived relative to the time resolution will have less intensity in the filtered ("gated") spectrum relative to the unfiltered (singles) spectrum.

Once an isomer had been identified the setup in Figure 9 was used to determine its lifetime. The SCA now is used to gate on the peak in the energy spectrum thought to be emitted by an isomer. The output from the SCA filters the time spectrum from the TAC, which is recorded.

The decay curve can be fit with exponentials by the method of least squares. The result is the half-life in channels. To calibrate the MCA in time units, the position of the prompt peak can be measured as a function of the delay of the BPO pulse using the setup in Figure 9 with the linear gate open. The function is linear and the slope of the calibration line is the required result. Table 2 shows the calibration data for the niobium isomer measurements. The slopes, determined by the method of least squares, are 40.8 $\pm$ 2.0 nanoseconds per channel for the Nb^{92} measurement; .747 $\pm$ 2% nanoseconds per channel for the Nb^{94} measurement.

Table 2. TAC Calibration Data

Nb^{92}

Added delay	Peak position (channels)
0 μs	22.7
.2	26
1.0	45.9
2.0	81.0
3.28	101.6
4.53	132.8

Nb^{94}

Added delay	Peak position (channels)
300 ns	90
400	224
500	359
600	487
700	630
800	764
900	889

B.3. Results

The data for the measurement of the lifetime of the 222 keV state in Nb^{92} is shown in Figure 11a. This decay spectrum was obtained by gating on the 90.7 keV gamma ray, which is emitted in the decay of that state (see II.B.1). The large prompt peak is due to the continuum under the peak (see Figure 6) mostly the result of Compton interactions in the Ge(Li) detector by higher energy gamma rays. Reduction of the data was complicated by poor statistics and by a lack of a clear measure of the background. Ideally the background can be found by measuring the time spectrum over many half-lives. Unfortunately the longest time between beam bursts available (8 μsec) was of the order of the half-life.

The least-squares routine, FRANTIC,[19] indicated minimum residual for a single component fit with no background. Figure 11b, however, shows the time spectrum obtained by gating on all pulses whose energy was greater than 100 keV. The background is 10.1 ± 0.2 counts per channel. If we normalize the two spectra, using the number of events in the prompt peaks, we find the background in the upper spectrum to be 17 ± 2 counts per channel. From Table 3, this yields a half-life of 128 ± 14 channels, or 5.2 ± 0.7 microseconds. This value is in agreement with the value 5.9 ± 0.5 μs of Duffield and Vegors,[58] for an isomer of Nb^{92} discovered using the (γ,n) reaction. Ivanov *et al.*[59] recently reported a value of 7 ± 1 μs for an isomer of niobium produced by proton bombardment of natural zirconium (17% Zr^{92}).

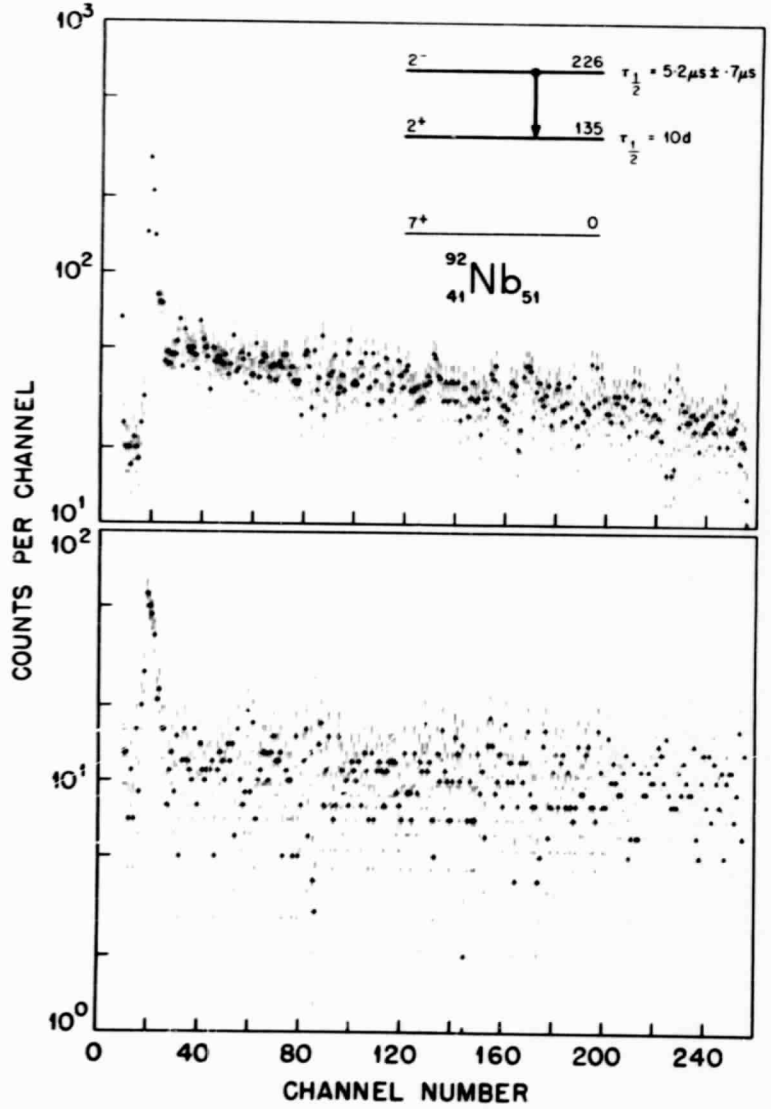

Fig. 11. (upper) The decay of the 90.7 keV Gamma Ray from the Reaction $Zr^{92}(p,n)Nb^{92}$; (lower) Random Coincidences; (inset) Partial Level Scheme of Nb^{92}.

Table 3. Half-Life of the 140.1 keV Level in Nb^{92} as a Function of Random Background Height

Background Counts per Channels	$\tau_{1/2}$ Channels	$\tau_{1/2}$ Microseconds
0	246 ± 16	10.0 ± 0.7
3.	244 ± 16	9.9 ± 0.7
1	239 ± 15	9.8 ± 0.6
3	225 ± 14	9.2 ± 0.6
10	176 ± 12	7.2 ± 0.5
15	142 ± 10	5.8 ± 0.4
17	128 ± 9	5.2 ± 0.4
18	121 ± 8	4.9 ± 0.3
19	114 ± 8	4.6 ± 0.3
21	100 ± 7	4.1 ± 0.3

The data for the measurement of the lifetime of the 140.1 keV level in Nb^{94} is shown in Figure 4. The decay spectrum was obtained by gating on the 99.404 keV gamma ray. There is no obvious prompt peak as in the Nb^{92} spectrum because the 99 keV line is much larger than background. Note that time now increases from right to left. Because the half-life of the 140 keV state is short compared to the time between beam bursts, the state decayed to background for which an unambiguous value could be found. The method of least squares again was used to yield a value of 49.2 $\pm$ 0.2 channels or 36.4 $\pm$ 0.8 nanoseconds. The inset in Fig. 4 shows the prompt peak. The shift between the maxima of the two distributions is real. It has been duplicated by folding a Gaussian shape into an exponential. Also this computer experiment proves that this folding does not alter the value of the half-life.

C. Experimental Details of E0 Measurement

C.1. Philosophy

As we have seen in Section I.C.2, the E0 branching ratio is a small number. Therefore the measurement of E0 electron decay from an excited 0^+ state requires a sensitive technique.

Let us first consider an experiment that measures the energy spectrum of electrons from Br^{80}. The counting rate is usually written[60] as

$$R_1(t) = (R_o e^{-t/\tau})\, f\, \omega_1\, \epsilon_1$$

where R_o is the initial disintegration rate of the source

f is the branching ratio for the mode of decay under investigation

ω is a solid angle efficiency factor

ϵ is an intrinsic efficiency factor

τ is the lifetime of the species.

If the source is counted for several half-lives, the total number of counts detected is, to a good approximation

$$N = \int_o^\infty R(t)\, dt$$

$$= R_o\, f\, \omega_1\, \epsilon_1\, \tau$$

From the decay scheme in Figure 3 it can be seen that two kinds of distributions are expected. The beta decay produced a continuous distribution of electrons, whose density slowly varies with energy. The internal conversion process however produces a line spectrum. Thus detection of the E0 transition means the detection of a peak on a smooth background.

The number of E0 electrons detected can be calculated using, for Kr^{80}, $f = 2\,\mu \times 10^{-3}$ where μ is the ratio of the number of E0 electrons to E2 photons decaying from the 0^+ state. For Br^{80m} τ is 2.34×10^4 sec. $(R_o\, \omega_1\, \epsilon_1)$ is the initial detector count rate, which we assume to be 10^4 sec^{-1}. Therefore $N_{E0} = 4.68\,\mu \times 10^5$. The background, i.e. the continuum the peak is sitting on, may be calculated using tables of the Fermi function[61] to be 1.0% of the total beta decays of this branch assuming 20 keV resolution.

Therefore $f = (0.0104)(0.85) = 8.8 \times 10^{-3}$ and $N_{background} = 2.0 \times 10^{6}$. We can "see" a peak on the continuum if its area is greater than background statistics. Therefore our sensitivity is such that we measure μ if $\mu > 3 \times 10^{-3}$.

The sensitivity may be increased by capitalizing on the fact that the 1306 keV E0 is in coincidence with the preceding beta ray while the 2.0 MeV ground state beta ray is non-coincident. Therefore consider detecting beta-conversion electron coincidences. The real coincidence rate is given by

$$R_{12} = R\, f_1\, f_2\, \omega_1\, \omega_2\, \varepsilon_1\, \varepsilon_2$$

and the background random rate by

$$R_c = 2T\, R^2\, f_1\, f_2\, \omega_1\, \omega_2\, \varepsilon_1\, \varepsilon_2$$

where

$$R = R_o\, e^{-t/\tau}.$$

We will consider the beta ray to be detected in counter 2, the E0 line in counter 1. Now $f_1 = \mu$, $f_2 = 2 \times 10^{-3}$ so that $N_{12} = \int_0^\infty R_{12}\, dt = 2.8\, \mu \times 10^{4}$ assuming $R\, \omega_2\, \varepsilon_2 = 10^{4}$ sec^{-1} and $\omega_1\, \varepsilon_1 = 0.05$. For a chance coincidence anything can trigger counter 2 so that $f_2 = 1$, $f_1 = 8.8 \times 10^{-3}$ as before and

$$W_c = \int_0^\infty R_c\, dt = 3.05 \times 10^{2}$$

assuming $2T = 15$ ns and $R\, \omega_1\, \varepsilon_1 = 10^{4}$ sec^{-1}. Using our significance criterion we must have $N_{12} \geq \sqrt{N_c}$ which means our sensitivity is $\mu > 6 \times 10^{-4}$. Note that this value is <u>independent</u> of initial count

rate. This value can be improved on by repeated experiments. For n measurements as above the sensitivity is $\mu > 12n^{-1/2} \times 10^{4}$. Thus by requiring coincidences between the E0 electron and the beta ray, the sensitivity has been improved by a factor of five.

C.2. Experiment

To implement the proposed measurement, the setup shown in Figure 12 was used. To measure the E0 electron energy spectrum the output of the Si(Li) detector was amplified, shaped, and stored in the MCA. To determine whether the coincidence requirement was met the time spectrum was measured using a TAC. This spectrum was filtered in the LG so that only time pulses were stored for which the energy from the plastic detector indicated that an energy of 700 keV or less was deposited. The two-parameter multichannel analyzer stored sequentially: (1) energy singles for the Si(Li) detector; (2) the gated time spectrum; (3) the coincidences between these two spectra.

Sources of Br^{80} were produced by irradiating a few tenths of a milligram of enriched $NH_4\, Br^{79}$ in the Oak Ridge Research Reactor for about twenty minutes. The 20 minute Br^{80g} activity was allowed to decay to its equilibrium value before the start of the experiment. The Br^{82} activity, originating from the 0.25% impurity of Br^{81} in the original sample was typically 0.1% of all activity at the start of a run and 1% at its termination. Altogether 80 runs were made with various parameters such as the timing and source strength altered in an attempt to improve accuracy. Some of these runs were

taken using an anthracene scintillation detector instead of the Si(Li), in an attempt to trade timing resolution for energy resolution. The final analysis was performed on a series of 19 runs. The best results were found using the seven runs with the lowest counting rates.

The energy scale was calibrated using Bi^{207} at regular intervals. Drift appeared to be less than 0.5 channels or 2.7 keV. The time scale was calibrated by inserting a calibrated delay line between the plastic TPO and the TAC. The result was 6.7 nanoseconds per channel. The efficiences of the two detectors given by the product $\omega\varepsilon$ was found by counting the Bi^{207} source in the same position as the Br^{80}. The Si(Li) efficiency for 1 MeV electrons is 1.5%, the plastic is 8%.

The spectra analyzed to give the final result are shown in Figure 13. The spectrum Y-PLANES 0 is the Si(Li) singles energy spectrum; Y-PLANES 30-49 represent energy spectra of pulses not in true coincidence. The spectrum Y-PLANES 10-15 represent energy spectra in true coincidence. The last spectrum shows the results of subtracting the "randoms" from the measured true coincidence spectrum to get the real coincidence spectrum. The energy calibration is 5.224 keV per channel with a bias level of 230 keV for channel 0. Thus the center of the E0 electron peak is expected to be in channel 206. It appears that within statistical uncertainties, there is no peak. Summing channels 204 through 207--a 20 keV window, yields 102 $\pm$ 10 counts. The random coincidence

47

taken using an anthracene scintillation detector instead of the Si(Li), in an attempt to trade timing resolution for energy resolution. The final analysis was performed on a series of 19 runs. The best results were found using the seven runs with the lowest counting rates.

The energy scale was calibrated using Bi^{207} at regular intervals. Drift appeared to be less than 0.5 channels or 2.7 keV. The time scale was calibrated by inserting a calibrated delay line between the plastic TPO and the TAC. The result was 6.7 nanoseconds per channel. The efficiences of the two detectors given by the product $\omega\varepsilon$ was found by counting the Bi^{207} source in the same position as the Br^{80}. The Si(Li) efficiency for 1 MeV electrons is 1.5%, the plastic is 8%.

The spectra analyzed to give the final result are shown in Figure 13. The spectrum Y-PLANES 0 is the Si(Li) singles energy spectrum; Y-PLANES 30-49 represent energy spectra of pulses not in true coincidence. The spectrum Y-PLANES 10-15 represent energy spectra in true coincidence. The last spectrum shows the results of subtracting the "randoms" from the measured true coincidence spectrum to get the real coincidence spectrum. The energy calibration is 5.224 keV per channel with a bias level of 230 keV for channel 0. Thus the center of the E0 electron peak is expected to be in channel 206. It appears that within statistical uncertainties, there is no peak. Summing channels 204 through 207--a 20 keV window, yields 102 $\pm$ 10 counts. The random coincidence

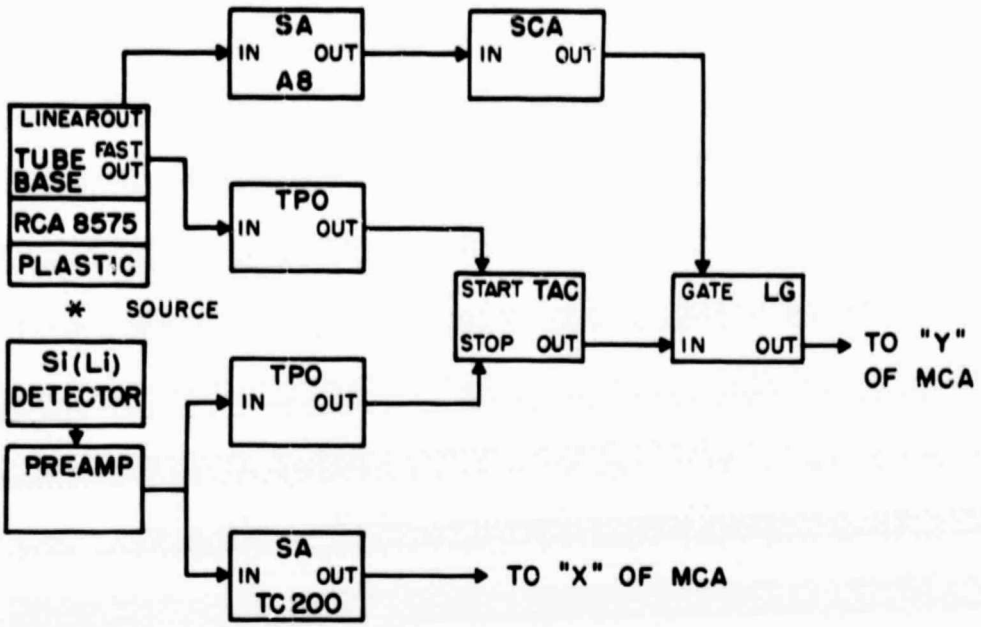

Fig. 12. Schematic of Electronic Setup for Krypton EO Transition Search.

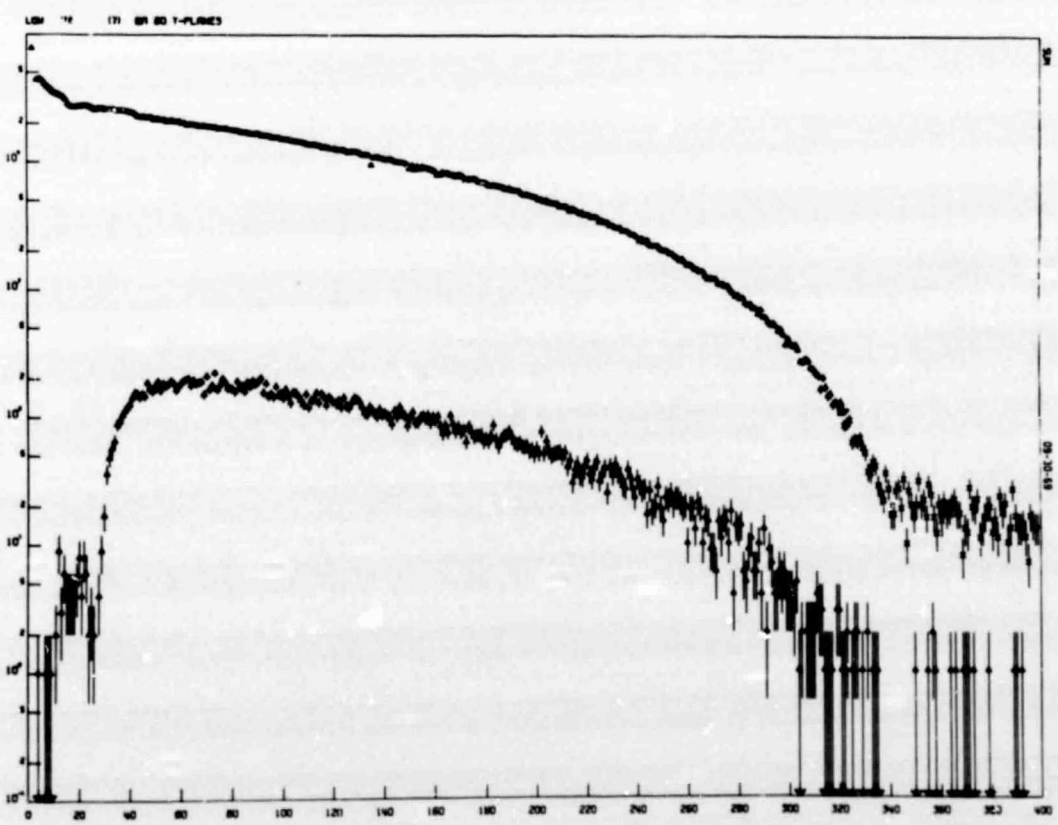

Fig. 13. Data for Krypton EO Transition Search: (a) (upper) Y-PLANES (0); (b) (lower) Y-PLANES (30-49.

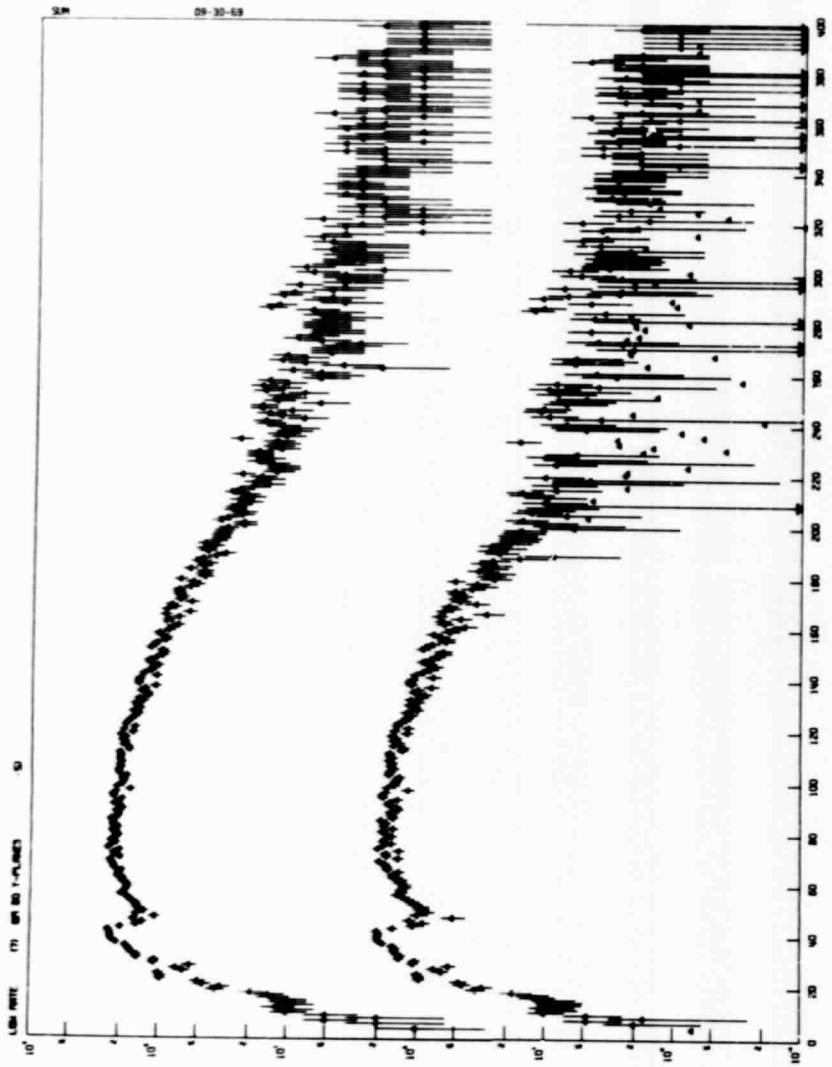

Fig. 13. (continued) (c) (upper) Y-PLANES (10-15);(d) (lower) Y-PLANES (10-15) - 0.3 * (30-49).

contribution is 65 ± 4.5 counts. Thus there are 37 ± 11 real coincidences in this window. Since a definite peak was not seen, these counts represent the background effects not associated with the EO transition. Thus the upper limit to N_{EO} is 11, the statistical uncertainty. To calculate μ the formula $N_{EO} = R\mu f_1 f_2 \omega_1 \epsilon_1 \omega_2 \epsilon_2$ will be used. Now the number of singles integrated over all energies is $R\mu\omega_1\epsilon_1$ where counter 1 is still the Si(Li) detector. This is found to be 5.2×10^7. f_2 is 2×10^{-3}, and the efficiency $\omega_2\epsilon_2$ is 0.06. Thus the upper limit on $\mu = f_1$ is 1.2×10^{-3}.

CHAPTER III. DISCUSSION AND SUMMARY

III.A.

In Section I.B.2. it was suggested that low-lying isomers in Nb^{92} and Nb^{94} might exist. Having shown they exist it may be asked, what is the significance of these values?

In Section I.B.2. it was noted that, from simple shell model considerations, these transitions are forbidden to be E1 or M2. Comparing the experimental numbers to the estimates in Table 1, it is seen that the half-lives are indeed much longer than the single-particle E1 prediction for both cases. In the Nb^{92} case the experimental number is also longer than the Weisskopf M2 value; in the Nb^{94} case, shorter. Since systematics show[68] that M2 transitions tend to be retarded, i.e., slower than single particle, we will consider the latter case to be a retarded E1. The former case will be discussed as E1 only, although the possibility of an M2 component exists. Only a measurement of the multipolarity of these transitions, such as by measurement of the conversion coefficient, can settle this matter.

Perdrisat[62] has recently published a "Survey of Some Systematic Properties of the Nuclear E1 Transition Probability." Following him we define the hindrance factor

$$H_w(E1) = \frac{B(E1)}{B_w(E1)} = \frac{T(E1)}{T_w(E1)} = \frac{\tau_{\frac{1}{2}w}(E1)}{\tau_{\frac{1}{2}}(E1)}$$

where T(E1) is the electric dipole transition probability, $B(E1) = T(E1)\,[E_\gamma^3\, A^{2/3}\ \text{sec}^{-1}]^{-1}$ is the reduced transition probability,* $\tau_{\frac{1}{2}} = .693/T$ is the half-life. The reference value is the Weisskopf[63] or single particle estimate, denoted by the subscript w. $B_w(E1) = 1.04 \times 10^{14}\ \text{MeV}^{-3}\ \text{sec}^{-1}$.**

In Table 4, the values of H_w for the niobium isomers are compared to the values of H_w for E1 transitions in nearby even-even nuclei. The value for Mo^{92} is calculated using the half-life of the 2612 keV state in Mo^{92}, and the branching ratio for the E1 and E2 decays from this state.[64] The value of H_w for Zr^{90} was calculated using the measured E2 to E1 branching ratio, assuming the E2 transition probability to be $4.6 \times 10^8\ \text{sec}^{-1}$--the Weisskopf value. Similar E2 transitions in this nucleus have been found to be slightly faster than single-particle estimates. Therefore H_w could be as great as 5×10^{-5} for this E1 transition.

The striking feature of these values of H_w is that the transition in Nb^{92} is considerably more hindered than the other three. A full scale shell model description of these states is presently being attempted, but the results will not be available for some time.[67] We can, however, in a very simple fashion consider an explanation for this. We will consider only proton excitations and will include only the possibility of impurities

---

*E_γ is measured in MeV.

**Lederer *et al.*[24] has $1.5 \times 10^{14}\ \text{MeV}^{-3}\ \text{sec}^{-1}$ because they use a different estimate of the nuclear radius.

Table 4. A Comparison of Several Hindrance Factors, H_w, for E1 Transitions Near A = 90

	$_{41}Nb^{92}_{51}$	$_{41}Nb^{94}_{53}$	$_{40}Zr^{90}_{50}$	$_{42}Mo^{92}_{50}$
$\tau_{1/2}$(exp)	6×10^{-6} s	36×10^{-9} s		1.50×10^{-9} s
$\tau_{1/2}$(E1)	6×10^{-6} s	36×10^{-9} s		18×10^{-9} s
E_γ(E1)	90.7 keV	99.404 keV	1136 keV	85 keV
E_γ(E2)			373 keV	329.3 keV
$I_i^{\pi_i} \rightarrow I_f^{\pi_f}$	$2^- \rightarrow 2^+$	$2^- \rightarrow 3^+$	$6^+ \rightarrow 5^-$	$6^+ \rightarrow 5^-$
% E1	100	100	97	9
α_{tot}(E1)	.14	.11		.18
T_w(E1)	1.6×10^{12} s^{-1}	2.1×10^{12} s^{-1}	3.1×10^{15} s^{-1}	1.4×10^{12} s^{-1}
H_w	6.3×10^{-8}	8.2×10^{-6}	$\geq 5 \times 10^{-6}$	2×10^{-5}

in one of the two states involved in the E1 transition. Writing down simple particle-hole excitations based on the most probable configurations for each state involved reveals that no orbit in the same proton shell ($f_{5/2}$, $p_{3/2}$, $p_{1/2}$, $g_{9/2}$) yield allowed E1 transitions. Going to the next shell lower ($f_{7/2}$) and the next shell higher ($d_{5/2}$, $g_{7/2}$, $h_{11/2}$, $d_{3/2}$, $s_{1/2}$) allowed E1 transitions can be found. For example, the $6^+ \rightarrow 5^-$ transition in Zr^{90} is forbidden for the configurations such as

$$(g_{9/2}^2)_{6^+} \rightarrow (p_{1/2}\, g_{9/2})_{5^-},$$

$$(p_{3/2}^{-1}\, p_{1/2}\, g_{9/2}^2)_{6^+} \rightarrow (p_{1/2}\, g_{9/2})_{5^-}, \quad \text{or}$$

$$(g_{9/2}^2)_{6^+} \rightarrow (f_{5/2}^{-1}\, p_{1/2}^2\, g_{9/2})_{5^-},$$

but allowed for

$$(g_{9/2}^2)_{6^+} \rightarrow (f_{7/2}^{-1}\, g_{9/2}^3)_{5^-},$$

$$(g_{9/2}^2)_{6^+} \rightarrow (h_{11/2}\, g_{9/2})_{5^-}$$

As can be seen only the $f_{7/2}$ hole and $h_{11/2}$ particle state appear to be effective in creating states decaying by allowed single particle transitions (though by no means have all states been written down). These same two orbits will also produce allowed E1 transitions in the Mo^{92} and Nb^{94} decays. For Nb^{92} however the basic forbidden transition is

$$[\pi\, p_{1/2}\, \nu d_{5/2}]_{2^-} \rightarrow [\pi\, g_{9/2}\, \nu d_{5/2}]_{2^+}$$

In this case, however, the configuration $[\pi\, h_{11/2}\, \nu d_{5/2}]$ couples only to 3^- through 8^-. So that only the $f_{7/2}$ configuration contributes:

$$[\pi(f_{7/2}^{-1}\, g_{9/2}^{2})\ \nu d_{5/2}]_{2^-} \rightarrow [\pi\, g_{9/2}\ \nu d_{5/2}]$$

The pickup and stripping reactions have revealed the major components of the wave functions of the low-lying states in the A = 90 region. The capture-gamma studies have shown the profusion of states that exist. Finally the $(p,n\gamma)$ isomer studies of retarded transitions seem to be capable of probing small and special components of the nuclear wave functions.

III.B.

In section II.C.2 a description has been given of the attempt to measure μ, the relative E0 transition probability in Kr^{80}. The upper limit measured, 12×10^{-4} is to be compared with the value calculated using Reiner's formulation, $4 \pm 1 \times 10^{-4}$. Therefore the sensitivity of the present measurement is not adequate to support or refute this prediction. The method proposed has reached its limit and could not be pushed farther. The difficulties included summing near the beta end point and backscatter coincidences because of the 180° geometry. If 180° geometry is not used, however, loss of solid angle causes an unacceptable reduction in counting rate. As was seen, the sensitivity of the coincidence experiment is independent of rate so that only by repeated experiments could accuracy be gained.

Suggestions for future research involve both theoretical and experimental approaches. Further calculations of μ should be done, especially with a microscopic model to provide a more realistic

prediction. Experimentalists will find several tools at hand to increase the sensitivity. Si(Li) detectors several times larger than the one used by this author are now commercially available and their use is (almost) routine. Magnetic steering devices have been recently developed that allow large solid angles (> 15%) and freedom from crosstalk between detectors. Multi-parameter analyzers, both hardware and software oriented, would allow the measurement of the coincidence time and both detector energies.

LIST OF REFERENCES

1. E. Rutherford, Phil. Mag. 21 (1911) 669.

2. H. Geiger and E. Marsden, Proc. Roy. Soc. (London) A82 (1909) 495.

3. H. Geiger, Proc. Roy. Soc. (London) A83 (1910) 492.

4. Nuclear Data Sheets, compiled by K. Way et al. (U. S. Government Printing and Publishing Office, National Academy of Sciences - National Research Council, Washington, D. C., 1958-1965); Nuclear Data, edited by K. Way et al., A1-, B1- (Academic Press, New York and London, 1966-).

5. M. A. Preston, Physics of the Nucleus (Addison-Wesley Publishing Company, Reading, Massachusetts, 1963) Part V.

6. W. M. Elsasser, J. Phys. Radium 4 (1933) 549, 5 (1934) 635.

7. M. Goeppert-Mayer, Phys. Rev. 75 (1949) 1969.

8. O. Haxel, J. H. D. Jensen, H. E. Suess, Phys. Rev. 75 (1949) 1766.

9. Preston, op. cit., p. 161.

10. K. H. Bhatt and J. B. Ball, Nucl. Phys. 63 (1965) 286.

11. J. Vervier, Nucl. Phys. 75 (1966) 17.

12. R. F. Sweet, K. H. Bhatt, J. B. Ball, Phys. Lett. 8 (1964) 131.

13. N. Auerbach and I Talmi, Nucl. Phys. 64 (1965) 458.

14. S. P. Pandya, Phys. Lett. 10 (1964) 178.

15. A. de-Shalit, Phys. Rev. 91 (1953) 1479.

16. S. Ramavataram, Phys. Rev. 135 (1964) B1288.

17. Y. E. Kim, Phys. Rev. 131 (1963) 1712; thesis, University of California, Lawrence Radiation Laboratory, Berkeley, Report No. UCRL-10865, 1963.

18. R. K. Sheline, C. Watson, E. W. Hamburger, Phys. Lett. 8 (1964) 121.

19. P. C. Rogers, Massachusetts Institute of Technology Laboratory for Nuclear Science, Technical Report No. 76.

20. J. B. Ball, M. R. Cates, Phys. Lett. 25B (1967) 126.

21. U. Gruber, R. Koch, B. P. Maier, O. W. B. Schult, J. B. Ball, K. H. Bhatt, R. K. Sheline, Nucl. Phys. 67 (1965) 433.

22. R. K. Sheline, R. T. Jernigan, J. B. Ball, K. H. Bhatt, Y. E. Kim, J. Vervier, Nucl. Phys. 61 (1965) 342.

23. E. J. Jurney, H. T. Motz, R. K. Sheline, E. B. Shera, J. Vervier, Nucl. Phys. A111 (1968) 105.

24. C. M. Lederer, J. M. Hollander, I. Perlman, Table of the Isotopes (John Wiley and Sons, Inc., New York, 1967) p. 578.

25. G. Scharff-Goldhaber, Phys. Rev. 90 (1953) 587.

26. E. Eichler, Rev. Mod. Phys. 36 (1963) 809.

27. G. H. Fuller and V. W. Cohen, Nucl. Data A5 (1969) 433.

28. A. K. Kerman and O. M. Shakin, Phys. Lett. 1 (1962) 151.

29. D. Mitra and M. K. Pal, Phys. Lett. 1 (1962) 153.

30. A. S. Reiner, Nucl. Phys. 27 (1961) 115.

31. A. S. Davydov, V. S. Rostovsky, A. A. Chaban, Nucl. Phys. 27 (1961) 134.

33. A. Bohr and B. R. Mottelson, Mat. Fys. Medd. Dan. Vid. Selsk. 27, No. 16 (1953).

34. R. L. Robinson, F. K. McGowan, P. H. Stelson, W. T. Milner, R. O. Sayer, Nucl. Phys. A124 (1969) 553.

35. F. K. McGowan, R. L. Robinson, P. H. Stelson, J. L. C. Ford, Jr., Nucl. Phys. A113 (1968) 529.

36. F. K. McGowan, R. L. Robinson, P. H. Stelson, J. L. C. Ford, Jr., Nucl. Phys. 66 (1965) 97.

37. J. J. Simpson, D. Eccleshall, M. J. L. Yates, N. J. Freeman, Nucl. Phys. A94 (1967) 177.

38. R. G. Stokstad, I. Hall, G. D. Symons, J. de Boer, Nucl. Phys. A92 (1967) 319.

39. P. H. Stelson, W. T. Milner, J. L. C. Ford, Jr., F. K. McGowan, R. L. Robinson, Bull. Am. Phys. Soc. 10 (1965) 427.

40. T. Tamura and T. Udagawa, Phys. Rev. 150 (1966) 783.

41. A. S. Reiner, Physica 23 (1957) 338.

42. E. L. Church and J. Weneser, Phys. Rev. 103 (1956) 1035.

43. N. P. Heydenburg, G. F. Peiper, C. E. Anderson, Phys. Rev. 108 (1957) 106.

44. G. B. Beard, Phys. Rev. 145 (1966) 862,

45. A. V. Ramayya, J. H. Hamilton, B. van Nooijen, N. R. Johnson, Phys. Rev. 157 (1967) 1015.

46. P. H. Stelson and L. Grodzins, Nucl. Data 1 (1965) 21.

47. P. H. Stelson, in Low Energy Nuclear Research, edited by D. M. van Patter and J. B. Marion (Academic Press Inc., New York, 1967) p. 141.

48. C. D. Moak, W. M. Good, R. F. King, J. W. Johnson, H. E. Banta, J. Judish, W. M. du Preez, Rev. Sci. Instr. 35 (1964) 672.

49. J. M. Blatt and V. F. Weisskopf, Theoretical Nuclear Physics (John Wiley and Sons, New York, 1952) Chapter VIII.

50. Ibid., p. 397.

51. R. L. Watson, private communication.

52. Blatt and Weisskopf, op. cit., p. 359.

53. For example see E. Eichler, P. H. Stelson, J. K. Dickens, Nucl. Phys. A120 (1968) 622.

54. E. Eichler, G. Chilosi, N. R. Johnson, Phys. Lett. 24B (1967) 140.

55. E. Eichler, J. K. Dickens, I. R. Williams, R. J. Silva, R. A. Kuetbing, ORNL-4164, p. 19.

56. Obtained from the Isotopes Division, Oak Ridge National Laboratory.

57. Hans Bichsel, University of Southern California, Department of Physics, Linear Accelerator Group, Technical Report No. 2, 1961.

58. R. B. Duffield and S. H. Vegors, Jr., Phys. Rev. 112 (1958) 1958.

59. E. A. Ivanov, A. Iordachescu, G. Pascovici, Rev. Roumaine Phys. 13 (1968) 879.

60. A. H. Wapstra, in Alpha, Beta, Gamma-Ray Spectroscopy, edited by Kai Siegbahn (North-Holland Publishing Company, Amsterdam, 1965) pp. 539-555.

61. U. Fano, Tables for the Analysis of Beta Spectra, National Bureau of Standards Applied Mathematics Series Handbook 13, p. 13.

62. C. F. Perdrisat, Rev. Mod. Phys. 38 (1966) 41.

63. V. Weisskopf, Phys. Rev. 83 (1951) 1073.

64. J. Konijn, E. W. A. Lingeman, P. F. A. Goudsmit, F. Diederix, B. J. Meijer, K. E. G. Löbner, Progress Report, Instituut voor Kernphysisch Onderzoek, Amsterdam, 1967-1968, p. 24.

65. J. M. Jaklevic, C. M. Lederer, J. M. Hollander, Phys. Lett. 29B (1969) 179.

66. J. B. Ball, J. B. McGrory, R. L. Auble, K. H. Bhatt, Phys. Lett. 29B (1969) 182.

67. K. H. Bhatt, J. B. Ball, private communication.

68. Nuclear Data Sheets, loc. cit., Section 6-6.